Pergamon

Int. J. Multiphase Flow Vol. 23, No. 6, pp. 1189–1209, 1997

Printed in Great Britain

PII: S0301-9322(97)00033-5

0301-9322/97 $17.00 + 0.00

EXPERIMENTAL STUDY OF THE PARTICLE FLOW IN A CIRCULATING FLUIDIZED BED USING A PHASE DOPPLER PARTICLE ANALYSER: A NEW POST-PROCESSING DATA ALGORITHM

T. VAN DEN MOORTEL, R. SANTINI, L. TADRIST and J. PANTALONI

Laboratoire de l'Institut Universitaire des Systèmes Thermiques Industriels (IUSTI), UMR 139 Université de Provence, Technopôle de Chateau Gombert, 5 rue Enrico Fermi, 13453 Marseille Cedex 13, France

(Received 15 August 1996; in revised form 24 April 1997)

Abstract—This study focused on the measurement of solid mass flux in the riser of a CFB cold pilot. The investigations were carried out using a Phase Doppler Particle Analyser (PDPA). Inconsistencies in PDPA results were observed when investigating flows with high particle densities. It appears that the performance of the measuring technique was affected by the optical thickness of the measured medium, thus producing substantial overestimation of the global solid phase quantity (e.g. solid mass flux). To determine the origin of these inconsistencies, the measuring system was subjected to complete recalibration. It was found that in flows with high particle densities, noisy Doppler signals tend to be split into several parts by the burst detector system, thus producing inconsistencies in the number of particles counted. The parameters associated with the splitting events were analysed, and a post-processing algorithm was developed to limit PDPA measuring errors. The aim of the post-processing algorithm was to rebuild the data and to recover the original measurements. The reconstitution process was applied to solid mass flux measurements in a CFB cold pilot. © 1997 Elsevier Science Ltd.

Key Words: gas–particle flow, Phase Doppler Particle Analyser, circulating fluidized bed, mass flux measurements

1. INTRODUCTION

A number of studies have been carried out to gain a better understanding of gas–solid flow in circulating fluidized beds. In these systems, different-sized particles are evacuated through a vertical riser under the effect of a gas flow. Depending on the operating parameters of the CFB (e.g. superficial gas velocity, properties of gas and solid particles, solid size distribution, size and shape of experimental device), different flow regimes can be obtained. Different concentration zones can be observed moving up and down the riser. Near the air distributor, the solid particles are thoroughly mixed and their volume fraction is high. The particles are ejected from the dense zone in the upper part of the riser and the mean particle concentration decreases moving toward the top of the riser. Numerous researchers (Rhodes & Laussmann 1992, Brereton & Grace 1993) have found that the regimes characteristic of CFBs present a rapidly ascending dilute core zone surrounded by a slower-falling suspension near the walls (annulus zone).

Understanding the hydrodynamic properties of the two-phase flow in the CFB riser is the key to better design and operation for such systems. Local solid concentration and the solid-phase distribution in the riser can be expected to directly affect gas–solid reactions and heat transfer rates in CFB facilities. Directly exposed surfaces in the riser have often been observed to present erosion problems. Local solid mass fluxes are important in describing and analysing the behaviour of the solid flow in CFB risers. The particle transfer mechanisms between the core and the annulus region of the gas–solid flow must be understood before predictive models and improve CFB systems can be developed.

Few investigations of local solid mass flux have been reported in earlier works. Isokinetic sampling probes have been used mainly to measure local solid mass fluxes in CFB cold pilots

(Rhodes & Laussmann 1992, Herb *et al.* 1992). Using this intrusive approach, radial time-averaged solid flux profiles are established for different superficial gas velocities and solid recirculation rates. More recently, Aguillon *et al.* (1995) published a comparative study of non-isokinetic sampling probes for solid flux measurements in CFBs. Three different types of probes were used in identical conditions and the respective net solid flux profiles averaged over the cross-section of the riser are compared to the overall flowrate of the circulating solids.

The local heterogeneity of the gas–solid flow in fluidized flow regimes has led to the development of measuring techniques that are capable of characterizing the local two-phase flow. Tsuji *et al.* (1984) used a laser-Doppler velocimeter to analyse air and solid particle velocities in a vertical pipe two-phase flow. Phase Doppler particle analysers (PDPAs) have been used in the dilute zone of the CFB riser to determine solid size, velocity profiles and local mass fluxes (Tadrist & Cattieuw 1993, Azario 1995). The major advantages of the phase Doppler particle sizer are its non-intrusive nature and its ability to produce simultaneous particle size and velocity measurements. What is more, the PDPA also provides enough data to determine local solid number density, volume flux and mass flux values, provided that the density is known.

This measuring technique used in many applications is a powerful tool to characterize solid size and velocity fields, but errors above 100% have been reported regarding mass fluxes and solid concentrations. Numerous studies have been done in order to determine the sources of such errors. Improperly sized particles (Gréhan *et al.* 1991, Onofri 1995), incorrect number of particles validated or inaccurate reference area (Saffman 1987) were found to directly affect the accuracy of PDPA measurements. Mass flux measurements may be strongly dependent on the optical alignment and are also sensitive to changes in set-up parameters and especially photomultiplier gains (Lazaro 1991). These authors also analysed the accuracy of PDPA measurements in optically thick, high particle density flows.

The deviation of the results with respect to the real conditions increased with the optical thickness of the measuring zone; this deviation is characterized by the overestimation of global quantities (e.g. solid mass fluxes, solid particle density or size distribution).

More recently, considerable improvements have been realized to minimise such errors. Qiu and Sommerfeld (1992) developed the so-called *logarithmic mean signal amplitude method*. This method provides an accurate estimation of the dependent particle size cross-section of the measurement volume for arbitrary particle trajectories. A novel method for particle concentration and mass flux measurements was developed based on the *Integral Value Method* (IVM) and the use of a one-component phase Doppler anemometer (Sommerfeld & Qiu 1995). The principle of this method is to determine the spatial volume concentration of the dispersed phase with the amplitude and the integral intensity of the reflected and refracted light.

Among the suggestions to improve the accuracy of PDA measurements, the *Dual Mode PDA* was introduced combining a standard PDA arrangement with a planar PDA (Schöne *et al.* 1995). The specificity of this method is to compare droplet diameters (or phase differences) measured by the planar PDA and droplet diameters measured by the standard PDA to determine whether the measurements will be accepted or discarded.

A comparative study between the dual mode PDA and IVM method (Dullenkopf *et al.* 1996) performed with a counter-based PDPA revealed the high accuracy of the two methods in characterizing typical pressure swirl atomisers sprays. However, the determination of mass fluxes in dense sprays remained a problem.

In the present work, comparisons between local time-averaged mass flux measurement profiles from the PDPA and global measurements in the recirculation loop revealed deficiencies of the PDPA system in certain flow configurations. The aim of this study was to identify the mechanisms whereby the PDPA fails to give consistent results in the characterization of mass flux. The experimental set-up was entirely calibrated and a post-processing code was developed to prevent solid mass flux measuring errors.

The first paragraphs describe the experimental set-up and the measuring technique. The results of calibration experiments are presented and analysed. These results were used to develop the post-processing algorithm. The effectiveness of the post-processing was validated using solid mass flux measurements in the dilute zone of a CFB cold pilot.

2. MATERIALS AND METHODS

2.1. *Experimental set-up*

A fluidization loop typical of circulating fluidized beds was used for the present work (figure 1). A detailed description of this device was provided in an earlier study (Tadrist & Cattieuw 1993). The riser is 2 m high, with a $0.2 \times 0.2\ m^2$ square cross-section. A pump located at the outlet of the cyclone sucks the air (ambient temperature and pressure) through layers of closely-packed glass beads (thickness 200 mm). A square grid plate with 26 μm openings is placed immediately above the layers of packed beads. This air distributor supplies a uniform plug flow of gas to the riser, even if there are no fluidized particles. The solid particles are formed of glass spheres (density $\rho = 2400\ kg/m^3$). The mean diameter of the particles constituting the bed is equal to 120 μm with a standard deviation of $\sigma = 20\ \mu m$. The solid volume fraction used in these experiments was equal to 3% of the riser volume.

The solid particles are fluidized when the air passes through the distributor. A flow of suspended particles (specific flowrate according to operating conditions) is then sent to the cyclone. The solid particles are then separated from the gas. The pump releases the air into the atmosphere and the particles are recycled via the recirculation loop and reintroduced into the riser. The superficial gas velocity in the riser is measured using a flow meter. The particle solid recirculation rate is determined using a buffer vessel on the recirculation loop (time-averaged measurement).

2.2. *Measurement technique*

The behaviour of the mixture is characterized by measuring the sizes and the velocities of the particles using a phase Doppler particle-sizing technique. The phase Doppler particle analyser used in this study is an Aerometrics counter-based instrument. A detailed description of this instrument was given by Bachalo and Houser (1984). In the following, only the relevant aspects concerning mass flux measurements will be described. The geometrical properties of the PDPA system are summarised in table 1.

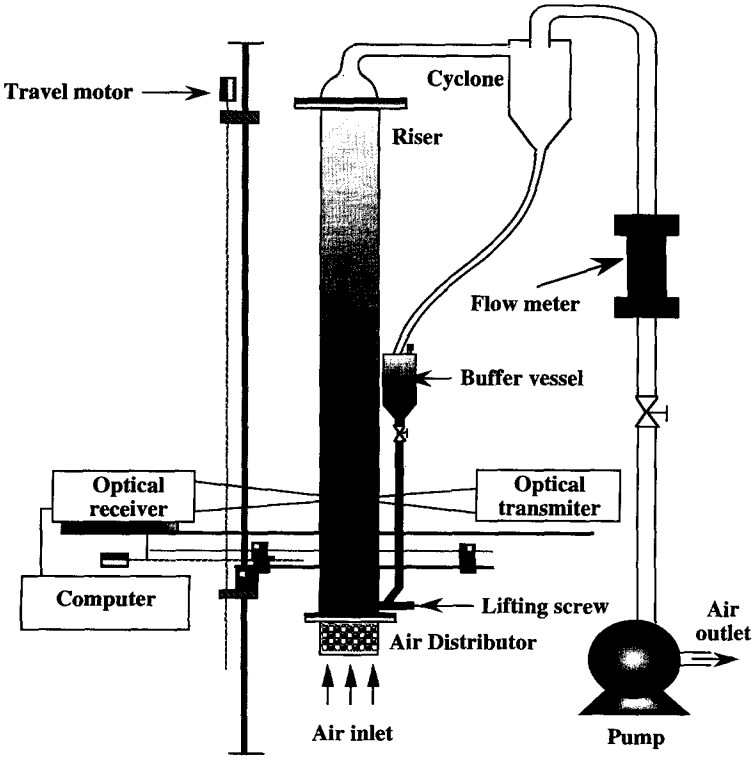

Figure 1. Schematic diagram of the circulating fluidized bed cold pilot set-up.

Table 1. Parameters of the PDPA optical system

Value	
Transmitting optics	
Wavelength of the laser (nm)	632.8
Diameter of the laser beam (mm)	2.1
Focal length (mm)	300
Beam separation (mm)	24
Beam crossing angle (°)	1.4
Diameter of measuring volume (μm)	176
Length of measuring volume (mm)	7.2
Number of fringes	13
Fringe spacing (μm)	13
Receiving optics	
Off axis angle (°)	30
Focal length (mm)	495
Aperature slit-width (μm)	100

This method is based on an optical system formed of a transmitter and a receiver identical to those used for conventional laser Doppler velocimetry. The difference resides in the placement of three detectors (at selected intervals behind the receiver aperture). This is a non-intrusive, off-scattering technique based on the analysis of the light scattered by spherical particles when illuminated by a coherent light source (a 10 mW He laser in this case).

The probe volume is located at the intersection of two laser beams emitted by the transmitter. At the overlap point of the two beams, an interference pattern can be observed and it is characterized by a set of illuminated fringes whose plane lies along the bisector of the two beams. An off-axis receiving lens transmits the cross-over point onto the set of photomultiplier tubes that form the detector. Each photomultiplier is placed to receive the far field scattering from the probe volume at slightly different angles.

When a particle passes through the fringes of the probe volume, the photomultipliers produce uniform Doppler bursts. A phase shift occurs between these bursts due to the slight difference in

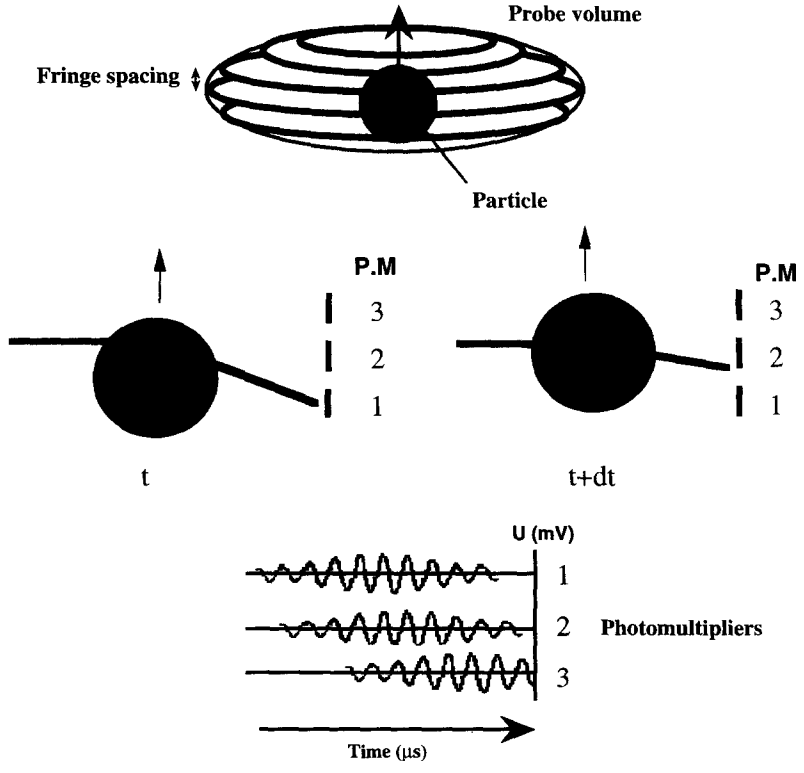

Figure 2. Doppler signals received on the different photomultiplier tubes corresponding to a single particle passing through the probe volume.

the collection angles of the different detectors (figure 2). Analysis of the Doppler signals can be used to indicate the size and velocity of each particle passing through the probe volume. Once a series of particles has been collected, different global quantities can be determined (e.g. solid mass flux or solid concentration). Before these quantities can be determined, the dimensions of the measuring probe must be established. Accurate determination of the measuring probe's dimensions is the most important step in the phase Doppler particle sizing technique.

*Particle velocity and particle size.*The frequency of each Doppler burst is proportional to the particle velocity component perpendicular to the plane of the fringes. The system used for this study allows a single velocity component to be measured. This component is defined as follows:

$$V_p = \frac{\lambda_0}{2 \sin\left(\frac{\Gamma}{2}\right)} F_D \qquad [1]$$

where λ_0 is the wavelength of the laser beam, F_D is the Doppler frequency, and Γ is the beam crossing angle.

It is possible to distinguish particles moving upward from those moving downward by setting a fringe velocity offset. The velocity offset is created by the rotating grating diffraction. This velocity is normally set so that the positive offset is opposite to the direction of the main particle flow (in this case the downward and upward respectively).

By analysing the relative shift between the signals from the different photomultipliers, we are able to determine the size of the particle. The phase shift is correlated to the particle size using a linear relationship derived from the calculation of the light refracted by a sphere that was proposed by Bachalo and Houser (1984). The particle diameter is determined as follows:

$$d_p = \frac{f\delta\Phi}{360\Delta l} H \qquad [2]$$

where f is the focal length of the transmitter lens, δ is the fringe spacing, Φ is the phase shift between two photomultipliers, Δl is the space between the detectors (1 and 3, or 1 and 2) and H is an optical constant.

The particle size and velocity readings are acquired during the measurement and stored in a computer file. Diameter and velocity ranges are respectively divided into 50 bins.

*PDPA global quantities.*Using the PDPA measuring technique, the first variables acquired are the Doppler frequencies, burst phase shifts and the number of fringes crossed by each particle moving through the probe volume. This data will indicate the particle size and velocity for each validated signal. When a given number of particles has been measured (i.e. acquisition time), several global variables are determined (Bachalo *et al.* 1988), including:

size and velocity distributions;
probe area/particle size correlation;
mean diameter and velocity of the distribution;
volume fluxes, mass fluxes;
solid number density.

*Signal detection/thresholding operation.*The PDPA measuring system uses log-amplified and filtered signals from the photomultipliers as input for the burst detection procedure. When the amplitude of the signal falls below a given value, the burst detector is switched off and the measurement is not validated. The disadvantage of this method is that the signal detection is based on a fixed amplitude threshold level. In consequence, difficulties may appear when investigating in variable flow conditions (e.g. variable solid concentrations). For this reason, special attention was paid in the present work for the application of appropriate amplitude threshold levels.

Note that various developments of signal detection methods have been progressively developed based on Fast Fourier Transforms (Domnick *et al.* 1988, Qiu *et al.* 1991; Ibrahim & Bachalo 1992, Qiu *et al.* 1994). These methods seem to improve frequency and phase estimations in complex two-phase flow measurements, but are not used in counter processors.

Characterization of probe volume.The Gaussian intensity distribution of the laser beams makes this determination somewhat complex. The probe volume can be considered cylindrical. It is now known that the sampling cross-section actually varies according to the size of the particle, the measuring conditions and the instrument set-up (Bachalo *et al.* 1988). Since the particles scatter an amount of light proportional to their squared diameter, and the detection presents a minimum signal threshold, the theoretical relationship between the probe diameter and the particle size is expressed as follows:

$$D^2_{(d_p)} = b_0^2 \ln\left(\frac{d_p}{d_{p\,min}}\right) + D^2_{min} \qquad [3]$$

where $D(d_p)$ is the probe volume diameter for the particle size d_p, D_{min} is the probe diameter corresponding to the minimum particle size $d_{p\,min}$ and b_0 is the $1/e^2$ beam waist.

Characterizing the dimensions of the probe volume based on an entirely empirical method would prove inaccurate. The increase in the dimensions of the probe volume with the photomultiplier voltage settings (PMV), the unpredictable variations in the intensity of the beams (due to light extinction by the solid particles) have a non-negligible effect on the actual probe area. The probe volume is thus determined using the PDPA program based on a semi-empirical approach (Bachalo 1990).

For each measurement, the number of fringes crossed by the particles is saved in a two-dimensional array. This array can be considered as a fringe-count histogram for each of the 50 diameter bins. For each diameter bin, the PDPA program determines the fringe count value with the highest number of hits. This value is multiplied by the fringe spacing which gives the experimental diameter $D'_{(d_p)}$ for each diameter bin. These values are then curve-fitted to the theoretical curve in [3]:

$$D'^2_{(d_p)} = 2k_1 \ln\left(\frac{d_p}{d_{p\,min}}\right) + k_2 \qquad [4]$$

Using the experimental values k_1 and k_2, the probe diameters can be calculated by rearranging [4] into:

$$D_{(d_p)} = \sqrt{2k_1 \ln\left(\frac{d_p}{d_{p\,min}}\right) + k_2} \qquad [5]$$

A slit aperture in the receiver controls the dimensions of the sampling cross-section. After the probe diameter $D_{(d_p)}$ has been calculated [5], it is multiplied by the receiver aperture S to determine the probe area for each diameter bin.

3. CALIBRATION OF THE MEASUREMENT SYSTEM

3.1. *Calibration set-up*

The calibration set-up is composed of a particle (known size) stuck onto a glass rod. The rod is then fixed on a rotating disk mounted on the shaft of a small variable speed motor (figure 3). This apparatus is mounted on the experimental device, on the same side as the receiving optics (figure 4). The position of the probe volume is adjusted to fall outside the CFB riser, so that when the motor is turned on the particle on the glass rod will rotate with the disk and pass through the measuring volume at a specified speed V_p. The trajectory of the particle through the probe volume is perpendicular to the plane forming the bisection of the two beams. This trajectory was manually adjusted to ensure that the particle would pass through the largest number of fringes.

The aim of the calibration system was to compare PDPA results in ideal and attenuated optical configurations. Variable density optical configurations were obtained by fluidizing the solid particles in the riser with different superficial gas velocities (U_g). Optical thickness conditions are then generated by the presence of the two-phase flow between the transmitter and the probe volume.

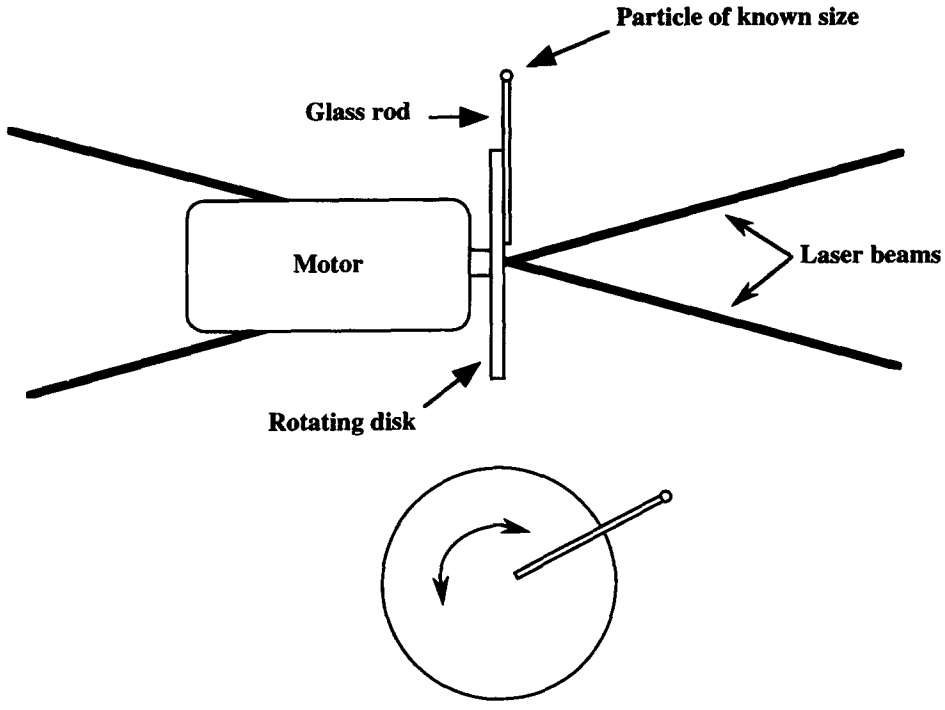

Figure 3. Schematic diagram of the PDPA calibration set-up.

When investigating turbulent two-phase flows, the range of light attenuation to which the laser beams are subjected before reaching the probe volume varies widely. This attenuation level depends on several parameters, including the particle size distribution, the number density or the optical path length through the medium. In general, the two-phase flow between the transmitter and the probe volume produces random intensity fluctuations of both laser beams crossing at the measurement point. These fluctuations normally increase with the attenuation level of the beams. The photomultiplier gains depend on the optical thickness conditions and must be adjusted for each measuring environment. The sensitivity of PDPA measurements to changes in photomultiplier voltages have been revealed by several authors (Lazaro 1991, Bachalo *et al.* 1988). It has been observed that for each measuring environment there is a corresponding working range of photomultiplier voltage values that will give accurate measurements.

In the Aerometrics system photomultiplier gain is not linear to photomultiplier voltage values. When a voltage V is applied between the cathode and the anode of a photomultiplier tube (photomultiplier voltage PMV), the current amplification or gain G_a is expressed as follows:

$$G_a = KV^{\omega n} \qquad [6]$$

where K is a constant, ω is a coefficient determined by the dynode material and geometric structure and n is the number of dynode stages characterizing each photomultiplier tubes. In figure 5 is reported the typical current amplification vs supply voltage law corresponding to the Aerometrics PDPA used for this study.

3.2. *PDPA performance in an ideal optical configuration*

An ideal optical measuring configuration is obtained when there is no attenuation of the laser beams before they reach the probe volume (figure 4(a)). The sensitivity of the PDPA measurements was analysed for different particle sizes and velocities. The dependence of global PDPA results on photomultiplier voltage settings is shown in figure 6(a)–(c).

It can be seen that the number of particles validated during the acquisition time presents a constant value for increasing PMV voltages (PMV < 350 V). At high PMV values (> 350 V), the signals produced by the particles passing through the probe volume were found to saturate the

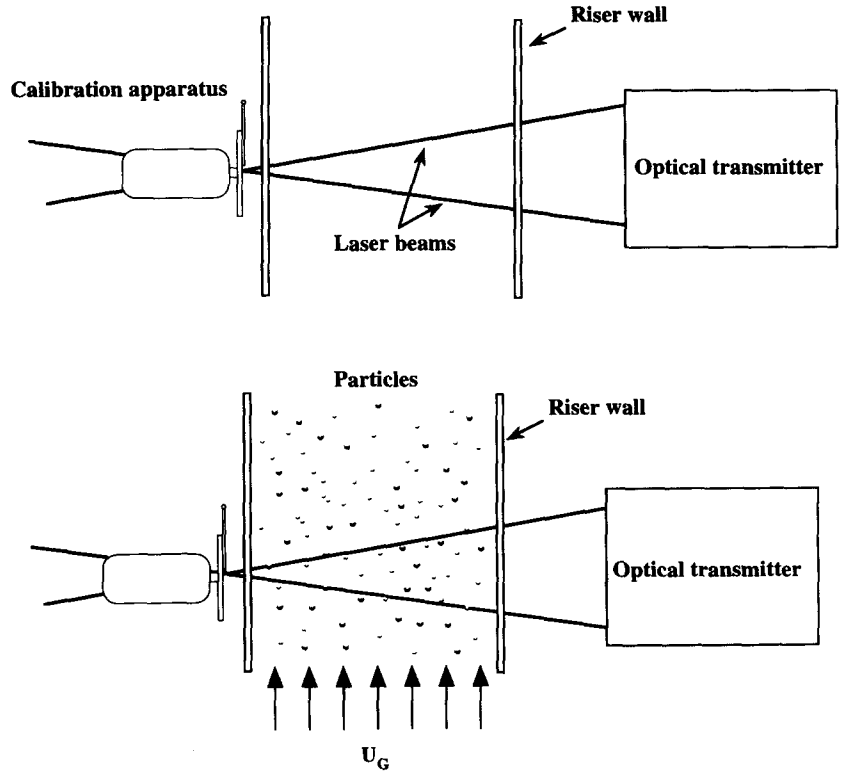

Figure 4. Schematic diagram of the calibration experiments in (a) an ideal optical configuration (no attenuation of the laser beams); (b) a high density optical configuration.

processor. The burst detection circuitry disregards those signals and the number of validated particles decreases as a consequence.

In the working range of photomultiplier voltages (260 V < PMV < 360 V), the mean particle

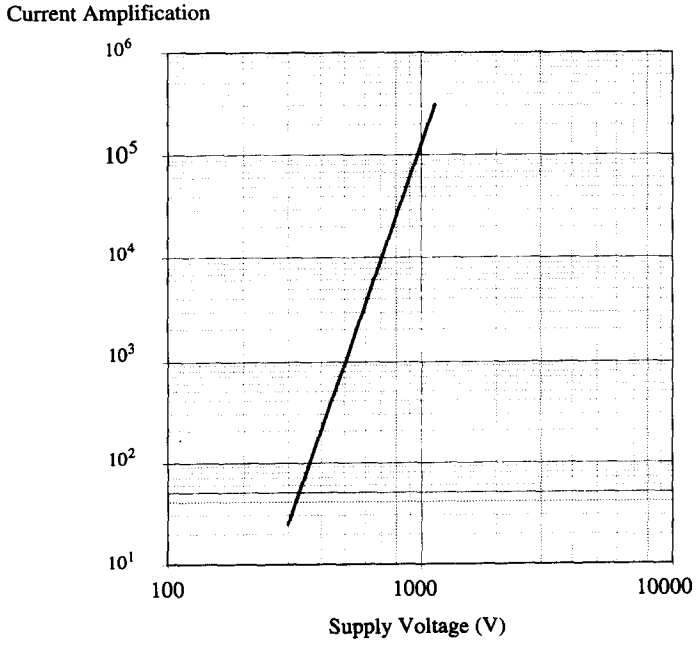

Figure 5. Typical current amplification vs supply voltage. Aerometrics system.

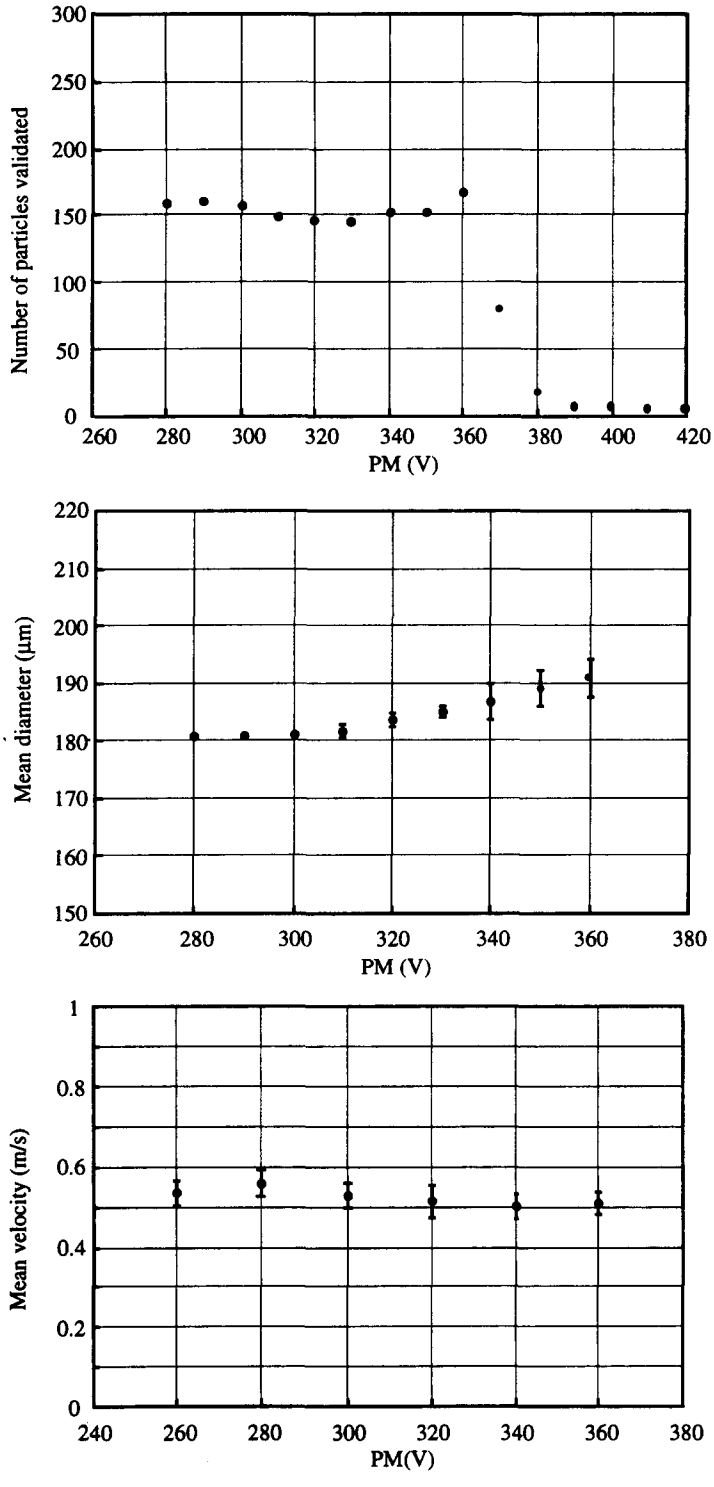

Figure 6. (a) Variation of the number of particles validated with the photomultiplier voltages. Ideal configuration $V_p = 1$ m/s, $d_p = 180$ μm. (b) Variation of the mean particle diameter (with associated standard deviation) with the photomultiplier voltages. Ideal configuration $V_p = 1$ m/s, $d_p = 180$ μm. (c) Variation of the mean particle velocity (with associated standard deviation) with the photomultiplier voltages. Ideal configuration $V_p = 1$ m/s, $d_p = 180$ μm.

velocity presents a nearly flat response with 10% maximum deviation, while the mean particle size response is seen to increase (low slope) with the increase in PMV values. This tendency is also observed for the mean particle size standard deviation.

The fringe statistics for a 180 μm particle diameter are given in figure 7 for three different photomultiplier gains. In this range of photomultiplier voltages, where the number of particles validated remains constant, the fringe crossing distributions present fairly uniform shapes. It can be seen that the peaks corresponding to the maximum number of fringes crossed by the particles increase progressively as a function of the photomultiplier voltages. This trend expresses the increase in dimensions of the probe volume with the sensitivity of the photomultiplier voltage settings.

3.3. *PDPA performance in attenuated environments*

For these experiments, the attenuation of the laser beams was generated by positioning the gas–particle flow between the transmitter and the probe volume (figure 4(b)). Three different attenuation levels were tested by progressively increasing the local solid volume fraction ϵ in the riser. Note that in our experiments, for all the different optical configurations tested, the attenuated length of the laser beams was kept constant. The dependence of global PDPA results on photomultiplier voltage settings is shown in figure 8(a)–(c).

When the solid concentration increases, the number of validated particles exhibits different behaviour patterns according to the photomultiplier voltage settings as follows:

—For PMV < 290 V, validated particle responses increase in a linear manner with low slopes. It can be seen that in this range of photomultiplier voltages the number of validated particles is slightly underestimated.

—For 290 V < PMV < 350 V, the measurements exhibit almost flat responses. In this range of photomultiplier voltages, all measurements merge to a single value. The results obtained are in good agreement with the results of the ideal configuration (maximum deviation 10%).

—For higher PMV (>350 V), the behaviour of the net mass flux responses changes completely. Experiments with $\epsilon = 0.4\%$ and $\epsilon = 0.65\%$ reveal considerable overestimation for the number of validated particles. The number of validated particles increases sharply as a function of the increasing PMV values. For a lower local solid volume fraction ($\epsilon = 0.23\%$), the number of validated particle responses is similar to that of the ideal configuration.

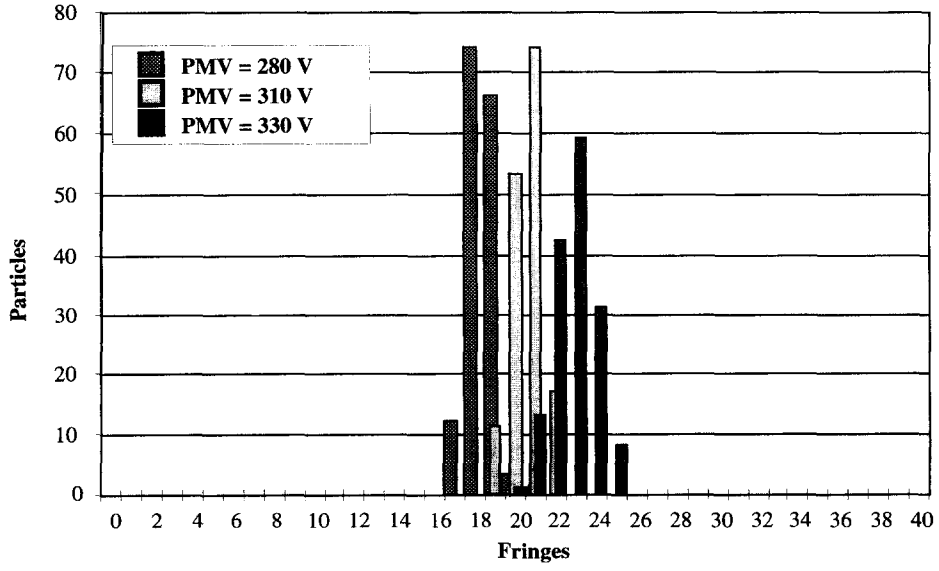

Figure 7. Fringe crossing statistics in the ideal configuration for three different photomultiplier voltages, $V_p = 1$ m/s, $d_p = 180$ μm.

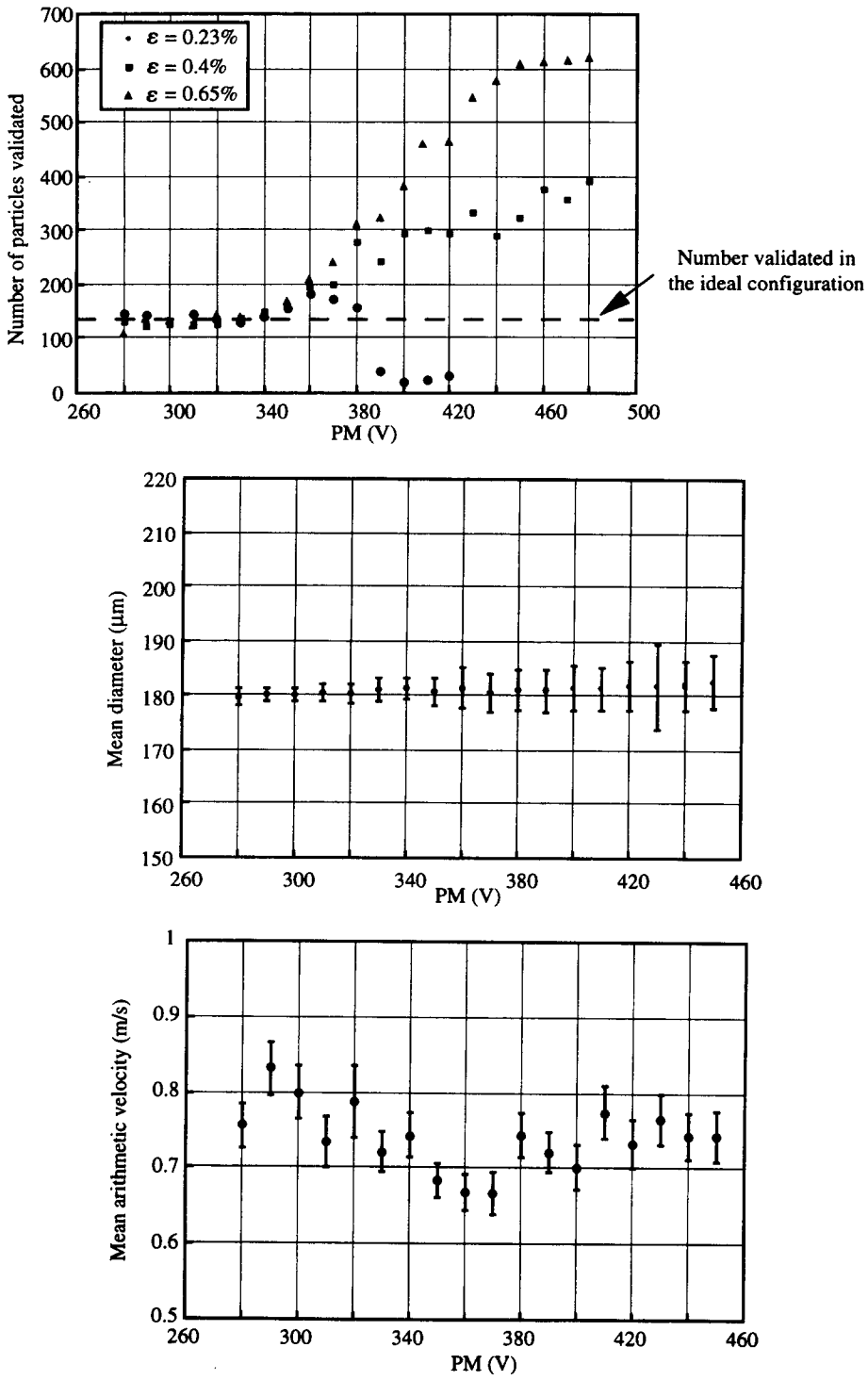

Figure 8. (a) Variation of the number of particles validated with the photomultiplier voltages in attenuated environments ($\epsilon = 0.23\%$, $\epsilon = 0.4\%$ and $\epsilon = 0.65\%$), $V_p = 1$ m/s, $d_p = 180$ μm. (b) Variation of the mean particle diameter (with associated standard deviation) with the photomultiplier voltages in an attenuated environment ($\epsilon = 0.65\%$), $V_p = 1$ m/s, $d_p = 180$ μm. (c) Variation of the mean particle velocity (with associated standard deviation) with the photomultiplier voltages in an attenuated environment ($\epsilon = 0.65\%$), $V_p = 0.8$ m/s, $d_p = 180$ μm.

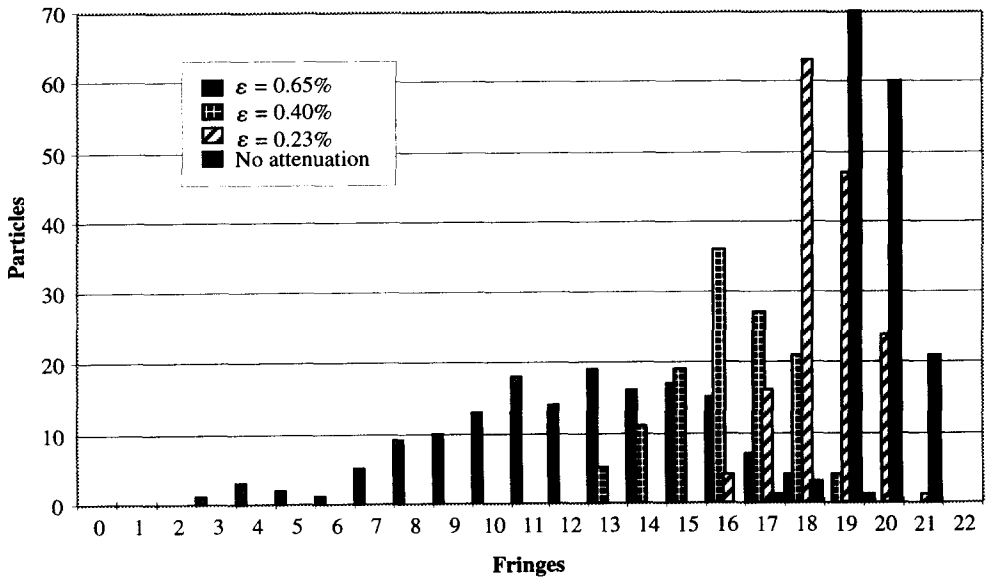

Figure 9. Fringe crossing statistics for a given photomultiplier voltage (PMV = 300 V) and for different attenuation levels of the laser beams, $V_p = 1$ m/s, $d_p = 180$ μm.

The particle size and velocity response results are slightly different from those obtained in the ideal configuration. Deviations of the results from the real values were observed principally for the anemometric results. It should be noted that the standard deviation of the particle size increases with the photomultiplier gain, yet the standard deviation of the mean velocity remains constant.

For a given photomultiplier voltage in the second range described above (i.e. 320 V < PMV < 350 V), it can be seen that the maximum number of fringes crossed by the particle decreases as a function of the solid concentration (figure 9). What is more, the increasing solid concentration produces wider distributions of crossed fringe values.

In the third range of photomultiplier voltages (PMV > 350 V), there is a decrease in the number of fringes crossed by the particle and a substantial increase in the number of particles validated during the 30 s period (figure 10).

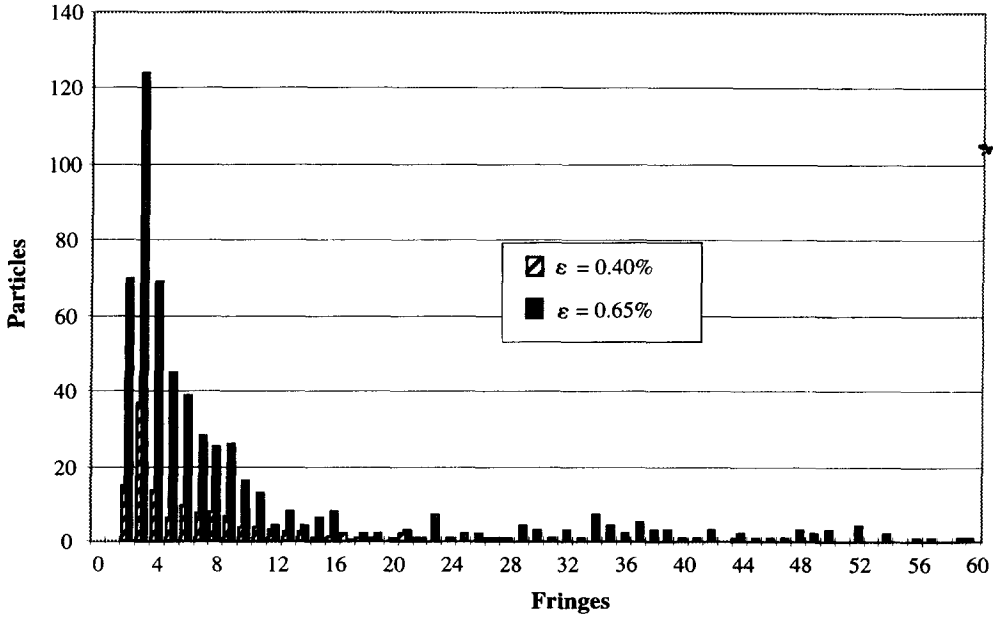

Figure 10. Fringe crossing statistics for a given photomultiplier voltage (PMV = 450 V) in attenuated environments ($\epsilon = 0.4\%$ and $\epsilon = 0.65\%$), $V_p = 1$ m/s, $d_p = 180$ μm.

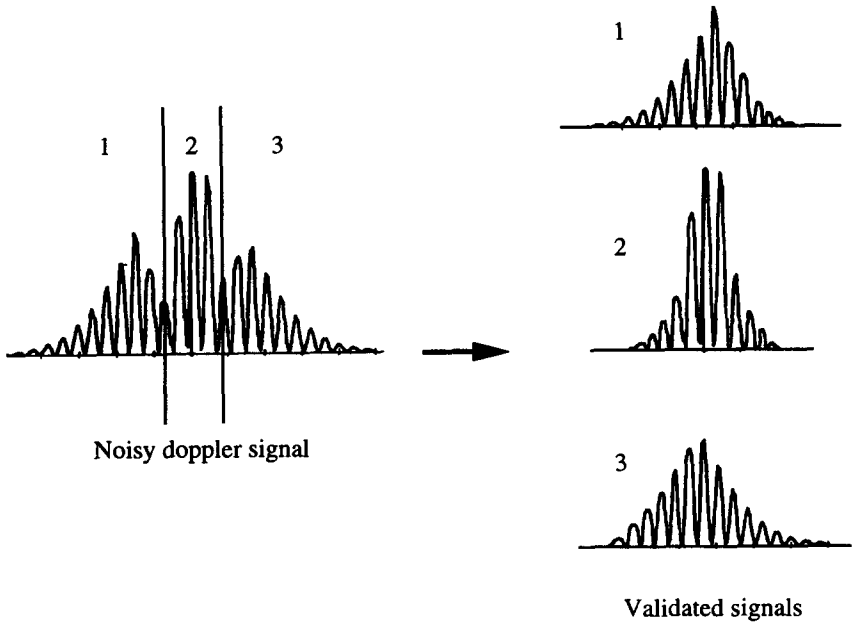

Figure 11. Burst splitting: example of a noisy Doppler signal split in three parts.

Overestimated particle counts correspond to a substantial decrease in the number of crossed fringes and to an increase in the width of the fringe crossing statistical distributions. The increase in the standard deviation of the fringe crossing distribution can be attributed to the non-correlated intensity fluctuations of the two beams. These fluctuations have a significant influence on the dimensions of the probe volume. For a given particle concentration, the fringe crossing statistical distributions shift to lower values as the photomultiplier gains increase.

From these observations, it seems that mass flux measurements are biased not only by the overestimation of the number of particles, but also by the changes in fringe statistics, both generated by beam attenuation levels and by photomultiplier gain settings. As described in section 2.2, determining the dimensions of the probe volume depends on the fringe statistics. Underestimating the number of crossed fringes has an immediate effect on calculated probe volume, thus generating significant overestimation of mass fluxes.

The analysis of the Doppler bursts produced in attenuated environments reveals significant deviation from ideal signal Doppler shapes. Instead of a theoretical Gaussian profile, the Doppler bursts are characterized by random fluctuations superposed on the Gaussian waveform (figure 11). This indicates that the intensity fluctuations of the laser beams (or the fringe pattern) occur within the time scale of an individual burst. A series of experiments revealed that the burst detector of the PDPA measurement system can be triggered several times by a single particle passing through the probe volume. As shown in figure 11, a noisy Doppler signal is treated as several Doppler signals similar in shape to the ideal Gaussian profile. Each fragmented Doppler signal contains the same size and velocity information about the measured particle (i.e. the same frequencies and phase shifts). What is more, the numbers of crossed fringes and the residence times are underestimated and they obviously decrease as the number of split signals increases.

As a result, this particle will be considered as several particles having almost the same size and velocity, passing the probe volume at very short time intervals. This explains the shift of the fringe statistics to lower values when the attenuation of the beams is increased. This 'Burst Splitting' phenomenon was also observed by Lazaro (1991), and it is very difficult to detect when investigating fluctuating two-phase flows.

*Influence of the particle velocity on PDPA measurements.*The same experimental set-up was used to test the influence of the particle velocity on PDPA measurement errors, notably on burst splitting events (see section 3.1). Several experiments were conducted to test a wide range of particle velocity

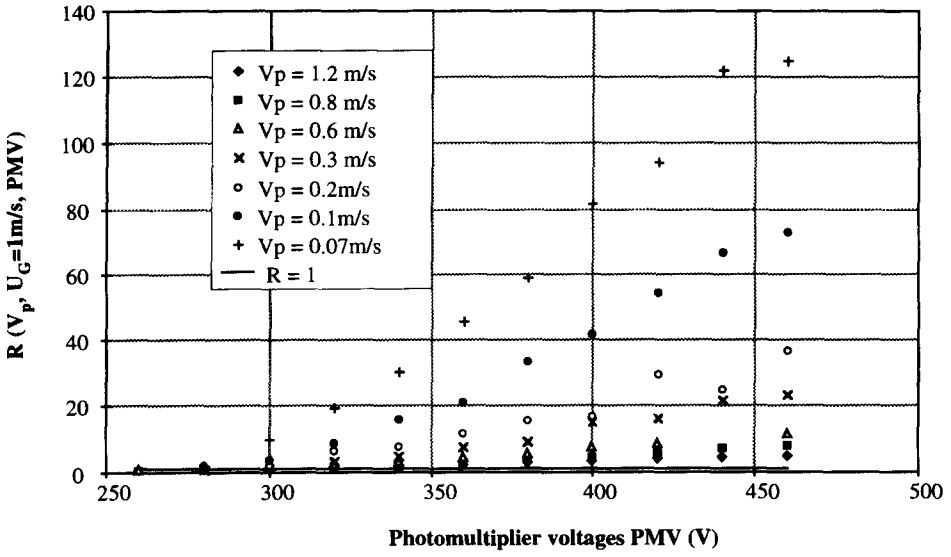

Figure 12. Variation of the deviation factor R for positive velocity values, $\epsilon = 0.65\%$, $d_p = 160\ \mu m$.

values. The sensitivity of the PDPA measurements was analysed according to photomultiplier voltage settings and then compared to the measurements for the ideal optical configuration.

The comparison was carried out for each experiment by introducing a deviation factor $R = R(V_p, \epsilon, \text{PMV})$ that compares the number of particles N detected under a given concentration to the number in the ideal case N':

$$R = R(V_p, \epsilon, \text{PMV}) = \frac{N}{N'} \qquad [7]$$

with $N = N(V_p, \epsilon, \text{PMV})$: number of particles validated per unit time under an attenuated environment for given particle velocity V_p, solid volume fraction ϵ and photomultiplier voltage PMV; $N' = N'(V_p)$: number of particles validated per unit time in the ideal configuration (no attenuation of the laser beams) for a given particle velocity V_p.

The number of particles validated in the ideal optical configuration N' was measured for each particle velocity V_p in the second range of PMV values (i.e. where PDPA global measurements show

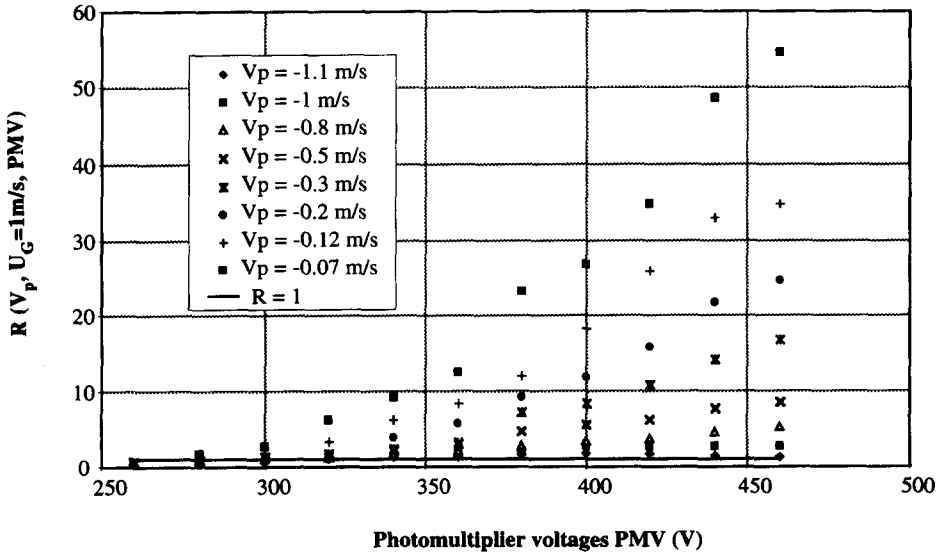

Figure 13. Variation of the deviation factor R for negative velocity values, $\epsilon = 0.65\%$, $160\ \mu m$.

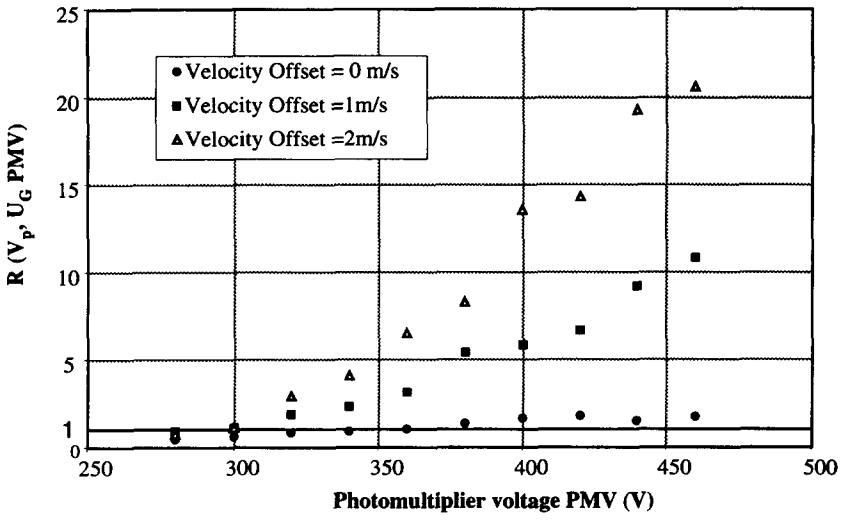

Figure 14. Variation of the deviation factor R for different velocity offset values, $\epsilon = 0.65\%$, $V_p = 0.3$ m/s, $d_p = 160$ μm.

flat responses). Figures 12 and 13 show the sensitivity of the R factor to changes in the photomultiplier gain settings for positive and negative values of the particle velocity V_p. On both graphs, it can be seen that for a given photomultiplier voltage, the R factor increases as the absolute particle velocity decreases. As an example, it can be observed that particle counts can be overestimated by a factor of 120 for $V_p = 0.07$ m/s and PMV = 460 V. These results confirm that burst splitting events are sensitive to the particle residence time in the probe volume. For the same absolute particle velocity, the positive velocity exhibits a higher R factor (about twice that of the negative value).

The differences observed concerning the sign of the particle velocity can be attributed to the fringe velocity offset. The fringes in the probe volume move opposite to the upward flow (i.e. the particles have positive velocity values). For a given absolute particle velocity value, the number of crossed fringes is therefore greater for the particle passing through the probe volume in a positive direction than one moving in a negative direction. The influence of the velocity offset value has been demonstrated using a fairly simple experimental approach.

*Influence of the velocity offset value on PDPA measurements.*Three experiments were carried out at an identical attenuation level of the laser beams ($\epsilon = 0.65\%$) and for $V_p = 0.3$ m/s, applying a different velocity offset value each time. The sensitivity of the R factor to changes in the photomultiplier voltages is reported in figure 14. These curves show that, for a given photomultiplier voltage, the R factor increases with the velocity offset value. It is important to note that when the fringes are stationary in the probe volume ($V_{offset} = 0$ m/s), the R factor response exhibits a nearly flat response (near $R = 1$).

Burst splitting events thus increase with the number of crossed fringes. In attenuated environments, the deviation of the Doppler signals from the ideal shape occurs during the time the solid particle crosses an illuminated fringe. The probability of obtaining a noisy Doppler signal will increase with the number of fringes crossed.

*Analysis of PDPA measurement errors.*All experimental results indicate that burst splitting is indeed the cause of the PDPA measurements errors in attenuated environments. The consequences of the burst splitting events are as follows:

—overestimation of the number of particles passing through the probe volume;
—a substantial deviation of the fringe statistics with respect to the ideal case, leading to a global underestimation of the probe area for each size bin.

These phenomena explain why the global mass fluxes were overestimated. What is more, the measuring errors increase with particle residence time in the probe volume. It is likely that velocity and size distributions can be biased for improper parameter settings.

4. POST-PROCESSING ALGORITHM

The parameters that cause measurement errors are often encountered in real CFB systems. The particles at a given location in the two-phase flow structure may present random trajectories through the probe volume (both upward and downward) with a wide range of velocity values. In such conditions, it is very difficult to detect and quantify measuring errors (since this requires extensive knowledge of the burst splitting events). An analysis of the temporal acquisition files was carried out for the experiments on the calibration apparatus.

4.1. *Time acquisitions*

The temporal files saved by the PDPA software have the structure described in table 2.Burst splitting events are easy to detect in calibration experiments, since a single particle of known size and velocity passes through the probe volume at constant time intervals. As the particle always has the same trajectory through the probe volume, the data saved in the temporal files should remain nearly constant.

Analysis of the data saved in attenuated environments shows that burst splitting events are characterized by small time intervals and particle residence times and by low fringe counts and signal intensities. No assumptions can be reliably advanced as to these sizes and velocity values.

4.2. *Reconstitution of the temporal files*

The amount of information available in the temporal files was sufficient to develop a post-processing algorithm for the biased data. This algorithm detects the burst splitting events in the temporal files. The original measurements are then reconstituted, by individually rebuilding the split signals. This reconstruction process is designed to correct the number of validated particles and to recover the data that characterizes Doppler bursts (numbers of crossed fringes, particle gate time).

Burst splitting detection in polydispersed two-phase flows.This detection relies on the validation of three criteria in the testing of the measurements (tested in pairs) saved in the temporal files. These criteria must be adjusted according to the experimental conditions (taking into account the solid size distribution, the superficial gas velocity, the range of measurable particle velocities and the intensity fluctuations to which the fringe pattern is subjected).

As was mentioned earlier in this paper, the burst splitting events are characterized by identical or very similar diameter and velocity values. In the case of polydispersed flows characterized by a solid size distribution, consecutive measurements with the same velocity and size values offered a good starting point for burst splitting detection.

These two criteria are then expressed as follows:

$$|d_{p_{i+1}} - d_{p_i}| < \epsilon_d \quad [8]$$

$$|V_{i+1} - V_i| < \epsilon_v \quad [9]$$

where ϵ_d and ϵ_v are constant values.

Table 2. Structure of the PDPA temporal raw files

Diameter	Velocity	Fringe count	Gate time	Intensity	Time intervals	Time
d_{pi}	V_i	F_i	G_i	I_i	Int_i	T_i
d_{pi+1}	V_{i+1}	F_{i+1}	G_{i+1}	I_{i+1}	Int_{i+1}	T_{i+1}
d_{pi+2}	V_{i+2}	F_{i+2}	G_{i+2}	I_{i+2}	Int_{i+2}	T_{i+2}

Fringe count: number of fringes crossed by the particle. If the velocity offset is switched on, the fringe count is corrected to determine actual fringes which would occur without velocity offset.
Gate time: particle residence time in the probe volume.
Intensity: signal intensity of the Doppler burst.
Time intervals: time intervals between the end of a measurement and the begining of the next one. During this time interval there are no particles in the probe volume.
Time: arrival time of each sample in the data run.

The determination of ϵ_v and ϵ_d must take into account PDPA configuration variables (i.e. probe volume dimensions, range of measurable sizes and velocities, measurement precision). To determine whether a pair of consecutive measurements originated from the same Doppler signal, a third criterion has been introduced based on fringe crossing statistics.

Before correcting the temporal files, the maximum number of crossed fringes Frg_{max} is determined for each particle size bin. The number of crossed fringes F_c from [12] that would result from the reconstruction of the two measurements (i and $i+1$) is compared to the Frg_{max} value (corresponding to the particle diameter d_{p_c} given by [11]. The third criterion is validated if the following condition is met:

$$F_c \leqslant Frg_{max}(1) \qquad [10]$$

where $Frg_{max}(1)$ is the maximum number of crossed fringes of the size bin 1, and 1 is the size bin corresponding to the corrected diameter d_{p_c} (if applicable). With

$$d_{p_c} = \frac{d_{p_i} + d_{p_{i+1}}}{2} \qquad [11]$$

and

$$F_c = \frac{\left[(G_i + G_{i+1} + \mathrm{Int}_{i+1} \times \left(\frac{V_i + V_{i+1}}{2}\right)\right]}{\text{Fringe spacing}} \qquad [12]$$

If the three criteria described above are not validated, the next two events to be tested will be $i+1$ and $i+2$.

Reconstruction of the temporal files. When two consecutive measurements have been validated and found to originate from a single particle passing through the probe volume, the correction algorithm will output a single measurement presenting the following characteristics.

Velocity:

$$V_c = \frac{V_i + V_{i+1}}{2} \qquad [13]$$

Diameter:

$$d_{p_c} = \frac{d_{p_i} + d_{p_{i+1}}}{2} \qquad \text{from relation [11]}$$

Corrected gate time:

$$G_c = G_i + G_{i+1} + \mathrm{Int}_{i+1} \qquad [14]$$

Corrected fringe count:

$$F_c = \frac{[G_c \times V_c]}{\text{Fringe spacing}} \qquad \text{from relation [12]}$$

Time interval:

$$\mathrm{Int}_c = \mathrm{Int}_i \qquad [15]$$

Time:

$$T_c = T_i \qquad [16]$$

The reconstruction of the measurements i and $i+1$ leads then to the corrected measurement c (table 3). After this reconstruction step, the next two events $i+2$ and $i+3$ are tested (burst splitting detection step again).

The entire data file can be corrected, by processing the burst splitting events in pairs. The whole temporal file is processed several times in order to detect and rebuild multiple burst splittings. The overestimated measurements are then corrected and the original fringe statistics are recovered.

Table 3. Structure of the PDPA temporal raw files after reconstruction of the events i and $i + 1$

Diameter	Velocity	Fringe count	Gate time	Intensity	Time intervals	Time
d_{pc}	V_c	F_c	G_c	I_c	Int_c	T_c
d_{pi+2}	V_{i+2}	F_{i+2}	G_{i+2}	I_{i+2}	Int_{i+2}	T_{i+2}
d_{pi+3}	V_{i+3}	F_{i+3}	G_{i+3}	I_{i+3}	Int_{i+3}	T_{i+3}

The corrected data files are then processed to determine the new global quantities that characterize the two-phase flow (solid mass fluxes, solid size distribution, etc.).

5. RESULTS

The efficiency of this post-processing program was tested for the case of a CFB cold pilot gas–particle flow. A series of experiments was carried out at different heights in the riser and for different solid flowrates to compare PDPA results for specific optical configurations. The solid mass flux measurements conducted on the PDPA technique are reported for normal use and after post-processing by specially-developed algorithms.

5.1. *Determination of solid mass flux in the CFB riser*

The PDPA optical measurement system described earlier is placed on a movable 3-axis base, allowing local measurements to be carried out at any height in the riser and at any location in the horizontal cross-section. A complete mapping can thus be produced for the local solid mass fluxes in the riser. Several experiments were conducted to analyse the variation in the axial solid mass flux profiles with the operating parameters of a CFB.

Local time-averaged net mass fluxes are obtained from the difference between upward and downward local solid mass fluxes:

$$\text{Net mass flux} = \text{upward mass flux} - \text{downward mass flux} \qquad [17]$$

At different heights in the riser, six different net mass flux profiles were reported. These profiles covered a quarter of the riser's cross-section (figure 15). At each height, the radial evolution of the local net mass fluxes was determined for two superficial gas velocities (0.9 and 1.1 m/s). Each

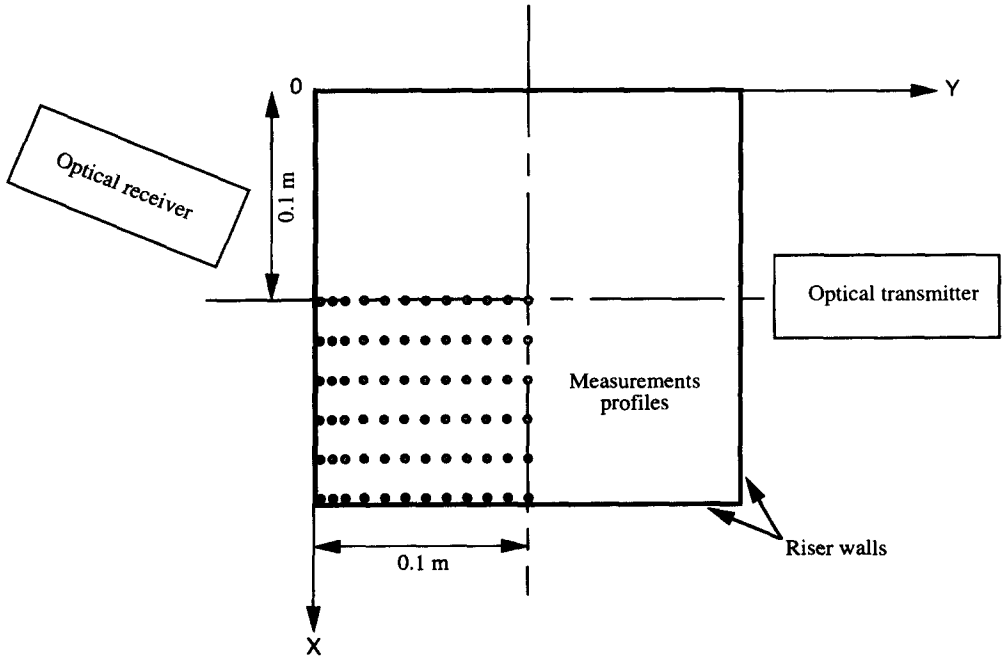

Figure 15. Schematic of the measurement profiles realised covering the quarter of the riser cross-section.

Table 4. Comparison of global net mass flux values between integrated PDPA and external measurements, elevation in the riser 120 cm

Superficial gas velocity (m/s)	PMV (V)	Net flux (kg/m² s) (PDPA)	Measured externally	Deviation
0.9	270	0.124	0.0825	51%
1.1	390	0.80	0.6	33%

radial profile in the study was obtained using a series of at least 12 individual net flux measurements (acquisition time 30 s).

These radial net mass flux profiles were integrated over a quarter of the cross-section of the riser using the trapezoidal rule. The integration result was extrapolated for the entire area of the column (axis-symmetric flow). The accuracy of the local measurements was tested by comparing the global net mass flux obtained by integration to the externally measured solid flowrate (accuracy 2%). Table 4 shows the experimental results 120 cm above the distributor plate for both superficial gas velocities.

These results reveal considerable overestimation of the global net mass fluxes reported by the PDPA measuring technique (i.e. compared to experimental values in the recirculation loop). Several methods of integrating the radial profiles were tested, and similar deviations were observed.

5.2. *Application of the post-processing algorithm*

The post-processing program was applied to each of the 12 temporal files constituting each radial profile. The criteria ϵ_d and ϵ_v were determined using the calibration experiments. In attenuated environments, with substantial burst splitting events, the variation laws for particle velocity and size standard deviations are independent of the imposed values. These deviations increase with the photomultiplier voltage level. The first two criteria were then selected as follows (for these experimental photomultiplier voltage ranges):

$$\epsilon_d = 10\ \mu\text{m} \quad [18]$$

$$\epsilon_v = 0.08\ \text{m/s} \quad [19]$$

Table 5 shows the results of the correction algorithm for the corresponding global net mass fluxes. In both cases ($U_G = 0.9$ and 1.1 m/s), the temporal files have been processed three times for global net mass fluxes to merge to these values.

The results of the corrected global net mass fluxes correlate quite well with the net mass flux measurements done on the recirculation loop.

Figure 16 shows the radial net mass flux profiles before and after the signal reconstitution. The same variation laws are observed in both cases. The time-averaged local net mass fluxes corresponding to the core of the two-phase flow present the largest deviations. The net mass flux profiles in the annulus zone (near the riser wall in the zone presenting negative net mass fluxes) were relatively unaffected by the post-processing.

Table 5. Comparison of global net mass flux values between integrated PDPA, external measurements and corrected PDPA measurements, elevation in the riser 120 cm

Superficial gas velocity (m/s)	Net flux (kg/m² s) (PDPA)	(PDPA) corrected	Measured externally	Deviation
0.9	0.124	0.0868	0.0825	5%
1.1	0.80	0.598	0.6	0.3%

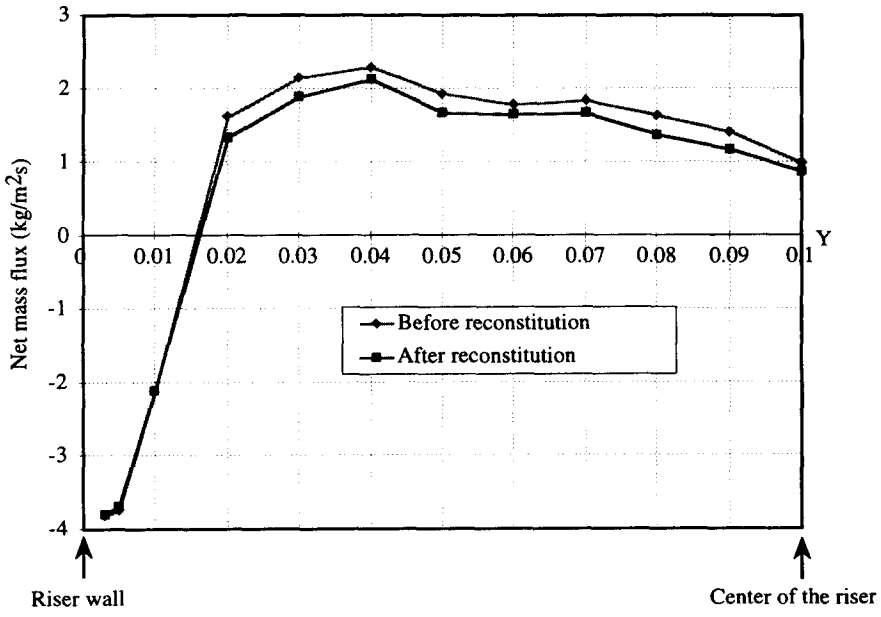

Figure 16. Net mass flux profiles before and after reconstitution of the temporal raw files, $U_g = 1.1$ m/s, $X = 0.1$ m.

6. CONCLUSIONS

The calibration procedure used in this study was developed specifically for the type of media encountered in CFBs. This approach allowed us to identify the limitations of the counter-based PDPA system and determine the typical causes of measurement errors obtained in complex and dense two-phase flows. It appeared that in optically thick configurations the Doppler signals tended to be split in several parts. A post-processing algorithm was developed to reconstitute the fragmented data in the initial temporal files. This processing was found to accurately indicate the number of particles that pass through the probe volume and to offer a better characterization of the probe's real dimensions. The post-processing algorithm offers reliable characterization of two-phase flows presenting wide size and velocity distributions, allowing researchers to investigate a much broader range of CFB regimes.

Acknowledgements—The authors would like to acknowledge ARENE (Marseille) and CNIM Co., Environment Department (La Seyne-sur-Mer) for their financial support.

REFERENCES

Aguillon, J., Shakourzadeh, K. and Guigon, P. (1995) Comparative study of non-isokinetic sampling probes for solids flux measurement in circulating fluidized beds. *Powder Technology* **83,** 79–84.

Azario, E., Tadrist, L., Pantaloni, J. and Cattieuw, P. (1995) Velocity analysis of the solid phase in circulating fluidized bed by using a phase Doppler particle analyser. *Proceedings International Symposium of the Engineering Foundation, Fluidization VIII.* Mat 14–19, Tours, France.

Bachalo, W. and Houser, M. (1984) Phase Doppler spray analyser for simultaneous measurements of drop size and velocity distributions. *Optical Engineering* **23(5),** 583–590.

Bachalo, W. D., Rudoff, R. C. and Brena, de la Rosa, A. (1988) Mass flux measurements of a high number density spray system using the phase Doppler particle analyser. *AIAA 26th Aerospace Sciences Meeting*, January 11–14, Reno, Nevada.

Bachalo, E. (1990) Proprietary information: Probe volume correction, November 5, Aerometrics Inc.

Brerton, C. M. H. and Grace, J. R. (1993) Micro structural aspect of the behaviour of circulating fluidized bed. *Chemical Engineering Foundation Science* **48,**(14), 2565–2572.

Dominick, J., Ertel, H. and Tropea, C. (1988) Processing of phase Doppler signals using the cross spectral density function. *Proc. 4th Int. Symp. on Applications of Laser Anemometry to Fluid Mechanics*, Paper 3.8.

Dullenkopf, K., Willmann, M., Wittig, S., Schöne, F., Stieglmeirer, M., Tropea, C. and Mundo, Chr. (1996) Comparative mass flux measurements in sprays using patternator and phase-Doppler technique. *Proc. 8th Int. Symp. on Applications of Laser Techniques to Fluid Mechanics*, Lisbon, pp. 20.1.1–20.1.8.

Gréhan, G., Gousbet, G., Naqwi, A. and Durst, F. (1991) Evaluation of a phase Doppler system using generalized Lorenz-Mie theory. *Int. Conf. on Multiphase Flow* '91, Tsukuba, Japan, pp. 291–296.

Herb, B., Dou, S., Tuzla, K. and Chen, C. (1992) Solid mass fluxes in circulating fluidized beds. *Powder Technology*, **70,** 197–205.

Ibrahim, K. M. and Bachalo, W. D. (1992) The significance of Fourier analysis in signal detection and processing in laser Doppler and phase Doppler applications. *Proc. 6th Int. Symp. on Applications of Laser Techniques to Fluid Mechanics*, Paper 21.5.

Lazaro, B. J. (August 1991) Evaluation of phase Doppler particle sizing in the measurement of optically thick, high number density sprays. United Technologies Research Center, East Hartford, Connecticut, UTRC91-11.

Onofri, F. (1995) Prise en compte de la dimension finie des faisceaux d'éclairage en granulométrie optique: Anémométrie phase Doppler. Diagnostics des milieux diphasiques. University of Rouen Ph.D. Thesis, France.

Qui, H. H., Sommerfeld, M. and Durst, F. (1991) High resolution data processing for phase-Doppler measurements in a complex two-phase flow. *Meas. Sci. Technol.* **2,** 455–463.

Qui, H. H. and Sommerfeld, M. (1992) A reliable method for determining the measurement volume size and particle mass fluxes using phase-Doppler anemometry. *Experiments in Fluids* **13,** 393–404.

Qui, H. H., Sommerfeld, M. and Durst, F. (1994) Two novel Doppler signal detection methods for laser Doppler and phase Doppler anemometry. *Meas. Sci. Technol.* **5,** 769–778.

Rhodes, M. J. and Laussmann, P. (1992) Characterizing non-uniformities in gas–particle flow in the riser of a circulating fluidized bed. *Powder Technology* **72,** 277–284.

Saffman, M. (1987) Automatic calibration of measuring volume size. *Applied Optics* **26,** 2592–2597.

Schöne, F., Tropea, C., Xu, T.-H. and Haugen, P. (1995) Mass flux measurements with phase Doppler anemometry. *Two-Phase Flow Modelling and Experimentation* 1995, pp. 751–757.

Sommerfeld, M. and Qui, H. H. (1995) Particle concentration measurements by phase-Doppler anemometry in complex dispersed two-phase flows. *Experiments in Fluids* **18,** 187–198.

Tadrist, L. and Cattieuw, P. (1993) Analysis of two-phase flow in a circulating fluidized bed. *Proc. 4th Int. Conf. on Circulating Fluidized Bed*, Vol. 2, pp. 702–707.

Tsuji, Y., Morikawa, Y. and Shiomi, H. (1984) LDV measurements of an air–solid two-phase flow in a vertical pipe. *J. Fluid Mech.* **139,** 417–434.